The Extracellular Potential of a Myelinated Nerve Fiber in an Unbounded Medium and in Nerve Cuff Models

Johannes Jan Struijk
Center for Sensory Motor Interaction, Aalborg University, DK-9220, Aalborg Øst, Denmark

ABSTRACT A model is presented for the calculation of single myelinated fiber action potentials in an unbounded homogeneous medium and in nerve cuff electrodes. The model consists of a fiber model, used to calculate the action currents at the nodes of Ranvier, and a cylindrically symmetrical volume conductor model in which the fiber's nodes are represented as point current sources. The extracellular action potentials were shown to remain unchanged if the fiber diameter and the volume conductor geometry are scaled by the same factor (principle of corresponding states), both in an unbounded homogeneous medium and in an inhomogeneous volume conductor. The influence of several cuff electrode parameters, among others, cuff length and cuff diameter, were studied, and the results were compared, where possible, with theoretical and experimental results as reported in the literature.

INTRODUCTION

Nerve cuff electrodes have been used for the recording of the electroneurogram (ENG) for more than 20 years (Stein et al., 1975; Hoffer, 1975). Recently this method was used for the first time in a chronic implantation in human subjects for the recording of signals from cutaneous afferents for the use of feedback signals in a system for the correction of foot-drop (Haugland and Sinkjaer, 1995).

Theoretical considerations and simple models have stimulated and accompanied the development of cuff electrodes. It has been known for a long time that the ENG could be recorded with higher amplitudes if the nerve and electrodes are lifted up into the air or into paraffin oil to provide a "locally restricted extracellular space." The analysis by Stein and Pearson (1971) of such a recording situation and its effect on the single fiber action potentials (SFAPs) was well applicable to nerve cuff electrodes (Stein et al., 1975). Further developments of models for the analysis of nerve cuff electrodes were published by Marks and Loeb (1976), who extended Stein and Pearson's model to the case of myelinated fibers, and by Stein and Oguztöreli (1978). In these analyses and models, assumptions were made that limit their applicability to the case of relatively long and narrow cuffs, with the electrodes not too close to the cuff's ends.

The first assumption was that the extracellular current is longitudinal, so that the membrane current density can be written as the derivative, with respect to the axial coordinate, of the extracellular current density. This requirement sets a lower limit to the length of the cuff, because the cuff must be longer than the rising phase of the transmembrane action potential (AP) (Stein and Pearson, 1971). This assumption also gave an upper limit to the cuff diameter for a given axial extent of the rising phase of the AP, and thus for a given fiber diameter.

The second assumption was that the potential at the cuff ends, because of the active fiber, is constant or vanishes. This again sets a lower limit for the minimum length-diameter ratio of the cuff. Except for the implications for the minimum length and minimum length-diameter ratio for which the analysis is still valid, the two assumptions also limit the minimum distance between one of the cuff ends and the electrode(s) that can be used in the analysis.

An attempt to lift the assumption that the extracellular current is strictly longitudinal was presented by Stein and Oguztöreli (1978). They used an analytical, cylindrically symmetrical volume conductor model to allow for radial extracellular currents. However, Heringa et al. showed that the use of the extracellular potential as a boundary value at the external surface of the fiber membrane, a method that was also used by Barker (1981), is inappropriate, although the consequences are "not intuitively obvious" (Heringa et al., 1989). However, in addition to the result of Heringa et al. that, in the case of extracellular voltage sources, additional sinks occur around the usual source-sink-source configuration, it is easy to imagine that in the case of multiple fibers unphysiologically large currents will flow between neighboring fibers because of these voltage sources.

Further developments of cuff electrodes and the quantitative analyses of recorded nerve signals require more sophisticated models to provide a solid foundation for these purposes. Such models should adequately describe the nerve fibers as electric sources, and they should comprise adequate volume conductor models, taking into account the properties of the nerve bundle and its surroundings, together with the cuff and its finite dimensions.

Nerve fibers (and, similarly, muscle fibers) as the sources of electric fields have received major attention in the literature. Classical publications by Hermann (1881), Lorente de

Received for publication 21 October 1996 and in final form 25 February 1997.

Address reprint requests to Dr. Johannes J. Struijk, Center for Sensory Motor Interaction, Aalborg University, Fredrik Bajers Vej 7D, DK-9220, Aalborg Øst, Denmark. Tel.: 45-96-35-8817; Fax: 45-98-15-4008; E-mail: jjs@miba.auc.dk.

0006-3495/97/06/2457/13 $2.00

Nó (1947), and Plonsey (1964) still form the background of many modeling studies in which the extracellular potential field of an unmyelinated nerve fiber is related to the intracellular or the transmembrane potential. Basically, in this formulation, the transmembrane current is given in terms of the intracellular and extracellular potentials and then used as a condition to relate extracellular and intracellular potentials, or equivalently, the extracellular potentials are related directly to the transmembrane potentials (note that this is a procedure different from the aforementioned incorrect application of a boundary condition on the external surface of the fiber). A similar procedure was used for myelinated fibers by Marks and Loeb (1976) and later by Ganapathy and Clark (1987) and Stephanova et al. (1989). The intraaxonal potentials were derived from empirical waveforms or calculated using Hodgkin-Huxley-like membrane kinetics, whereas the internodes were modeled as distributed cable models.

An alternative way of modeling the nerve fiber is to calculate the membrane current and use it as a current source in a volume conductor model. For unmyelinated fibers this current source is usually reduced to a line source (e.g., Heringa et al., 1989; Trayanova et al., 1990; see also Malmivuo and Plonsey, 1995), neglecting the radial extent of the fiber itself. In the model in the present work, the nodal currents are directly derived from the membrane kinetics at the nodes of Ranvier, and they serve as point current sources in a volume conductor model. Myelin currents are thereby neglected.

The volume conductor models have usually been models that could be described analytically, although a single numerical model has appeared in the literature (Barker, 1981). The analytical models are all based on cylindrical symmetry of the volume conductor. If there is a restriction (e.g., a cuff), then either this restriction is infinitely long (e.g., Heringa et al., 1989; Wijesinghe et al., 1991) or a simple boundary condition is applied at the cuff ends (Stein and Oguztöreli, 1978) to keep the mathematics manageable.

In the present work a numerical method was chosen to calculate the potential field inside a cylindrically symmetrical cuff. This allows for finite cuffs without any conditions at the cuff ends, and this method is very flexible in the sense that, within the constraint of axial symmetry, complex nerve and cuff geometries can be chosen.

METHODS

The model consisted of two parts. A fiber model was used to calculate the action currents at the nodes of Ranvier of the fiber, and the nodes were then regarded as current sources in a volume conductor model. First, an unbounded homogeneous volume conductor model (analytical model) was used to show the use of the fiber model and its differences as compared with models in the literature, and to use it as a reference model to show the influence of a more realistic volume conductor (including cuff electrode and fiber bundle). Second, an inhomogeneous volume conductor model of the nerve and cuff electrode is presented to show the influence of cuff length, cuff diameter, position of the electrode inside the cuff, etc. Third, a model similar to that of Marks and Loeb (1976) was used to show the value and the limitations of the one-dimensional approach.

Fiber model

The fiber model was a cable model, identical to the one used by Struijk et al. (1992) for electrical stimulation, except that the applied extracellular potentials were zero. In this model, the extracellular resistances were zero as well. However, the extracellular resistances were much smaller than the intracellular internodal resistances, and in the mathematical description of the model the extra- and intracellular resistances appear as a summation, so that the extracellular resistance can be neglected in the calculation of the transmembrane action potentials and action currents (FitzHugh, 1962). The nodal membrane kinetics were based on the work of Chiu et al. (1979) and some modifications by Sweeney et al. (1987). The main equations and the parameters used (at 37°C) are given in the Appendix. Integration of the differential equations was performed with a simple Euler integration with a step size of 0.1 μs.

With the parameters given, the conduction velocity of the AP was 55800 nodes/s. Because in the model the internodal distance L is proportional to the fiber diameter D ($L = 100D$), the conduction velocity v is $5.58D$, where v is given in m/s and D in μm. The factor 5.58 is close to the factor 6 that was derived from experimental data by Hursh (1939), whereas Schoonhoven and Stegeman (1991) summarized the data in the literature as "a conversion factor in the order of 5 (m/s)/μm at body temperature."

The linearity between v and D is not affected if the myelinated internodes in the model are modeled as a leaking cable, compared with a nonleaking internode. The influence of the internode on the proportionality and the question of whether the principle of "corresponding states" (Rushton, 1951) is preserved in a leaking cable were addressed in a study by Goldman and Albus (1968), and their positive answer is an important argument for the validity of the model used in the present study.

In Fig. 1 the AP and the nodal transmembrane current or action current (AC) are shown. The peak-to-peak current is 3.31 nA (maximum inward current 1.8 nA), which is in the lower end of the range of the nodal currents summarized by Marks and Loeb (1976). Note that the shape of the AC looks different from the one shown by Ganapathy and Clark (1987), the latter looking similar to the nodal ionic current, which is also shown in Fig. 1. The AC is the summation of the ionic current and the capacitive current (not shown).

The transmembrane current as shown in Fig. 1 was used as a template for the currents at all of the nodes in the model. The template was taken from node 11 of a 21-node fiber of 10-μm diameter. In the fiber model the amplitudes

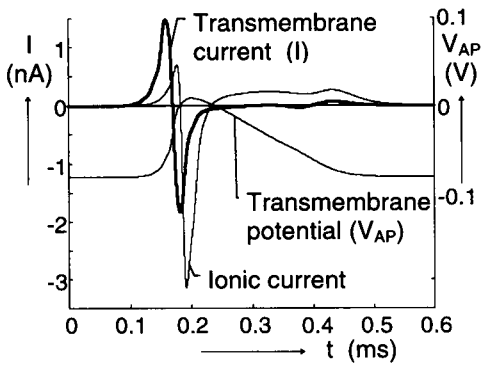

FIGURE 1 The nodal transmembrane current (used as a template in the fiber model), the ionic current, and the transmembrane potential (used in Eq. 6) as functions of time.

of the nodal currents are linear with fiber diameter, whereas the duration of the action current and the action potential are independent of fiber diameter. The template was scaled accordingly for different fiber diameters. The lengths of the fibers used in all volume conductor models was 500 mm, which was long enough, because the difference with a 250-mm fiber was approximately 1% in the worst-case situation of an electrode fiber distance of 100 mm. For smaller electrode fiber distances the error very rapidly decreased.

Unbounded homogeneous volume conductor

The single fiber action potentials were calculated with a 500-mm-long fiber at the z axis of a cylindrical coordinate system, where the central node of the fiber was at $z = 0$. The electrode was a point electrode at $z = 0$ and at radial distance $r = R$. A ring electrode with radius R at $z = 0$, centered at $r = 0$, gives identical results, which makes this model comparable with the inhomogeneous model described below. The conducting extracellular medium was unbounded, homogeneous, isotropic, and resistive, with a conductivity $\sigma = 1.0\ (\Omega\text{m})^{-1}$. The SFAP ($s(t)$) thus recorded is described by

$$s(t) = \sum_{n=1}^{N} \frac{i_n(t)}{4\pi\sigma\sqrt{z_n^2 + R^2}} \qquad (1)$$

where z_n is the z coordinate of node n ($z_{N/2} = 0$), N is the number of nodes, and $i_n(t)$ is the transmembrane current at node n. SFAPs were calculated as a function of fiber diameter D for different fiber-electrode distances r, and as a function of r for a given D.

Numerical accuracy

It turned out that the formulation of Eq. 1 can give rise to large errors if meticulous care is not taken that the time integral of $i_n(t)$ equals zero, as it should be.

In the first calculations the time integral of the SFAP turned out not to vanish, as it theoretically should (see Appendix A). For a 3-μm fiber of 500-mm length ($\sim$1667 nodes) and an electrode-fiber distance of 10 mm, the normalized error was -0.5, where the normalized error is defined as

$$\text{Error} = \int_{t_0}^{t_1} s(t)\mathrm{d}t \Big/ \int_{t_0}^{t_1} |s(t)|\mathrm{d}t$$

which should be zero. However, the time integral of the transmembrane current template was not zero either:

$$\int_{t_0}^{t_1} i_n(t)\mathrm{d}t \Big/ \int_{t_0}^{t_1} |i_n(t)|\mathrm{d}t = -8 \cdot 10^{-4}$$

which indicated a very small offset, due to numerical inaccuracies. Because of the large number of summations in Eq. 1, this offset grew to substantial values, especially for small fiber diameter and large R. Removal of the template offset yielded an error for the SFAP that was smaller than 0.01 (typically between 10^{-4} and 10^{-7}) instead of the original 0.5.

Inhomogeneous volume conductor

In Fig. 2 the inhomogeneous volume conductor is shown schematically. The length of the volume conductor was 500 mm and the height was 250 mm. At the upper, left, and right boundaries the potential was set to zero (Dirichlet boundary condition), whereas at the lower boundary (the axis) the normal current density was zero (Neumann boundary). The model consisted of a nerve bundle (fascicle) with a radius of 0.5 mm, a perineurium with a thickness of 50 μm, and a cuff with variable length and variable inner diameter. The thickness of the cuff material was always 1.0 mm. The conductivities are shown in Table 1 (see also Goodall et al., 1995).

The cuff's conductivity was varied in one simulation to estimate the influence of a leaking cuff. In the case of a split cuff where the cuff can be opened to put it around the nerve and then is closed, it may happen that the cuff is not perfectly closed, so that a small gap exists through which current leaks. This reduces the constrictive properties of the cuff. A way to simulate the current leakage in a cylindrically symmetrical model instead of using a full three-dimensional

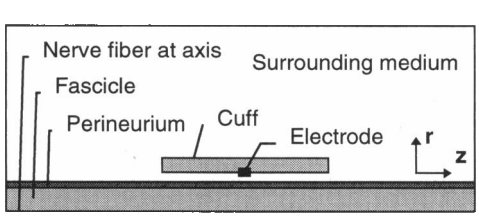

FIGURE 2 Schematic drawing of the volume conductor model (not to scale). Only the upper half of the model is shown; the lower boundary in the figure is the model axis.

TABLE 1 Conductivities

	σ_z(1/Ωm)	σ_r(1/Ωm)
Fascicle	0.6	0.083
Perineurium	0.0034	0.0034
Cuff	10^{-6}	10^{-6}
Surrounding medium	1.0	1.0

model is to change the conductivity of the cuff in such a way that the total radial cuff resistance equals the resistance of the gap. The resistance of a cylindrical cuff with inner diameter R, an outer diameter R_o, a length L_{cuff}, and a conductivity σ_{cuff} is given by

$$R_{cuff} = \frac{1}{2\pi\sigma_{cuff}L_{cuff}}\int_R^{R_o}\frac{dr}{r} = \frac{1}{2\pi\sigma_{cuff}L_{cuff}}\ln\left(\frac{R_o}{R}\right)$$

For the gap the resistance is given by

$$R_{gap} = \frac{2\pi R}{g}\left(\frac{1}{2\pi\sigma_{gap}L_{cuff}}\ln\left(\frac{R_o}{R}\right)\right)$$

where g is the gap width measured at the inside of the cuff wall, and σ_{gap} is the conductivity in the gap. For a given gap width, the corresponding cuff conductivity to simulate this gap can then be calculated by

$$\sigma_{cuff} = \frac{g\sigma_{gap}}{2\pi R} \tag{2}$$

Numerical aspects

In a cylindrically symmetrical volume conductor with cylindrically symmetrical current sources, the potential field can be expressed in two of the three cylinder coordinates (the radial coordinate r and the axial coordinate z) plus time t. If the sources $i_n(t)$ of the current are infinitely thin ring electrodes with radii R_n, or if they are nodes of Ranvier of a nerve fiber at the axis with radius R_n, and if the conductivity is anisotropic with a value of σ_r in the radial directions and σ_z in the axial directions, then the potential $u = u(r, z, t)$ can be written as

$$\left[\frac{\partial}{\partial r}\left(\sigma_r\frac{\partial}{\partial r}\right) + \frac{1}{r}\sigma_r\frac{\partial}{\partial r} + \frac{\partial}{\partial z}\left(\sigma_z\frac{\partial}{\partial z}\right)\right]u(r, z, t)$$

$$= -\sum_{n=1}^{N}\frac{i_n(t)}{2\pi R_n}\delta(r - R_n, z - Z_n) \tag{3}$$

where N is the number of ring-shaped sources, and Z_n is the z coordinate of source n.

Equation 3 can be solved analytically for simple geometries only. For the geometry as shown in Fig. 2 this is still possible in theory, but the expressions become extremely complex and time consuming to evaluate. Therefore, and to allow for more complex geometries, a numerical method was preferred.

A straightforward way of solving Eq. 3 would be to calculate the total source current distribution, i.e., the currents at the nodes of Ranvier, for instants $t = kT$, where T is the temporal sampling interval, and then calculate the field u for all k. To calculate a SFAP with a duration of 2 ms and a bandwidth of 5 kHz in this way would require a time window of $3 \times 2 = 6$ ms and a sample frequency of 10 kHz. This method then requires $10{,}000 \times 0.006 = 60$ times a solution of the whole volume conductor problem (Eq. 3). A compound action potential (CAP) of many fibers would take even more work: a superimposed source current distribution can be calculated, after which again for each time $t = kT$, the CAP can be calculated, but typically with a longer duration and thus with a higher number of required solutions of the volume conductor problem than for the SFAP.

Basically, this high number of required solutions is caused by the properties of the source. As follows from Eq. 3, $i_n(t) = i_0(t - n\Delta t)$, which means that the different currents are different functions of time, even though this is just a matter of time shifts, and therefore the solution $u(r, z, t)$ is not separable for the place-time variables, i.e., u cannot be written as $u(r, z, t) = U(r, z)T(t)$. Nevertheless, an alternative and much faster way of calculating the SFAP (or CAP) can be based on the fact that for a single node of Ranvier, Eq. 3 is separable: $u_n(r, z, t) = w_n(r, z)i_n(t)$. Superposition gives a SFAP, $s(r, z, t)$:

$$s(r, z, t) = \sum_{n=1}^{N} w_n(r, z)i_n(t) \tag{4}$$

This formulation gives the opportunity to use the lead field concept, based on the reciprocity theorem (see, e.g., Malmivuo and Plonsey, 1995), to reduce the amount of work: instead of calculating the potentials on an electrode due to activity of the nodes of Ranvier at the axis of the model, we can calculate the potentials at the nodes of Ranvier due to currents impressed on the electrode. Consequently, for a given monopolar electrode, or any given electrode configuration, the volume conductor problem had to be solved only once. The SFAP $s(t)$ as recorded at this electrode was then calculated as

$$s(t) = \sum_{n=1}^{N} w_n i_n(t) \tag{5}$$

where w_n is the lead field at node n and $i_n(t)$ is the transmembrane current at node n. This equation also holds for CAPs by interpreting N as the total number of nodes of all fibers. Note that Eq. 5 is the same as Eq. 1, except that w_n is now a much more complex function of the electrode position and of the nodal positions.

Equation 3 was solved where the right-hand side resembled a current impressed on the recording electrode, and thus the lead field was obtained. The SFAP was then calculated with Eq. 5. A finite difference method was used to calculate the lead field, because of the flexibility of the

method and the ease of incorporating finite anisotropic structures, the latter being impossible in, e.g., a boundary element method.

The method for calculating the potential field was slightly different from the one described by Rijkhoff et al. (1994) and is given in Appendix C. Equation C.5 was iterated in a pointwise red-black Gauss-Seidel manner, until the relative change of the potentials at the axis was not more than 10^{-7} per relaxation sweep. The number of grid points in the model was 269 × 170 = 45,730. The sizes of the cells varied from 0.125 × 0.025 mm^2 around the electrode to 5 × 5 mm^2 in the upper corners of the model.

One-dimensional analysis

Although a difference with Marks and Loeb (1976) was that in the present study the internode is not leaking, exactly the same mathematical analysis holds. It is only that the potential between the nodes had a linear shape instead of an exponential one. So, assuming that the extracellular currents as well as the intracellular currents are strictly axial, the transmembrane current can be written as

$$i_m = -\frac{1}{r_e}\frac{\partial^2 V_e}{\partial z^2} = \frac{1}{r_a}\frac{\partial^2 V_a}{\partial z^2}$$

where V_e is the extracellular potential, V_a is the intracellular potential, and r_e and r_a are the extracellular and intracellular resistances per unit length, respectively. Solving for V_e, with V, the membrane potential, defined as $V_a = V + V_e$, and with the extracellular potential set to zero at the cuff ends, the extracellular potential V_e inside the cuff is found as

$$V_e(t, z) = \frac{R_e}{R_e + R_a}\left[\left(1 - \frac{z}{L_{cuff}}\right)V(t) - V\left(t - \frac{z}{v}\right) + \frac{z}{L_{cuff}}V\left(t - \frac{L_{cuff}}{v}\right)\right] \quad (6)$$

where v is the propagation velocity; $V(t)$ is the transmembrane potential, which, for the nodes of Ranvier, is given in Appendix B by equation B.1, and between the nodes by a linear interpolation of the APs at the nodes; R_a is the intraaxonal resistance, as given by Eq. B.3; and, similar to Marks and Loeb (1976), R_e, the extracellular resistance, is given by

$$R_e^{-1} = \frac{2\pi}{L}\int_{r_{fiber}}^{r_{cuff}} \sigma_z r \, dr \quad (7)$$

Equation 6 was used to compare the one-dimensional analysis with the solution of Eq. 3 to estimate the cuff lengths, cuff diameters, and electrode positions inside the cuff for which the analysis in Eq. 6 is valid and those for which it breaks down.

RESULTS

Unbounded homogeneous volume conductor

SFAP amplitude

In Fig. 3 the peak-to-peak amplitude of the calculated SFAP is shown as a function of fiber diameter for three different electrode-fiber distances: R = 0.1 mm, R = 1.0 mm, and R = 10 mm. It was proposed in the literature that SFAP amplitude varies exponentially with conduction velocity v, or with a linear relationship between v and the fiber diameter D:

$$\hat{s}(D) \propto D^p \quad (8)$$

where the exponent p ranges from 1.0 (Erlanger and Gasser, 1937) to 3.22 (Rosenfalck and Ottosen, 1982), depending on various assumptions, but is typically taken to be 2.0, which is the value that follows from the core conductor model (e.g., Olsen and BeMent, 1981; Erlanger and Gasser, 1937; Buchthal and Rosenfalck, 1966; see also Schoonhoven and Stegeman, 1991, for an excellent overview).

In Fig. 3, with its double logarithmic scale, the exponent p is the slope of the curves. It is clear that p is not constant but depends on both the fiber diameter and the electrode-fiber distance. For a short distance and large fibers ($R \ll L$), $p \approx 1$. This result is explained by the linear relationship between the nodal action current and the fiber diameter. The potential field close to the node is proportional to the nodal current (field of a monopolar source). However, this holds only for this particular situation, where the electrode is at the same z coordinate as one of the nodes of Ranvier. For an electrode halfway between adjacent nodes, $p \approx 0$ for very small electrode-fiber distances (not shown in the figure).

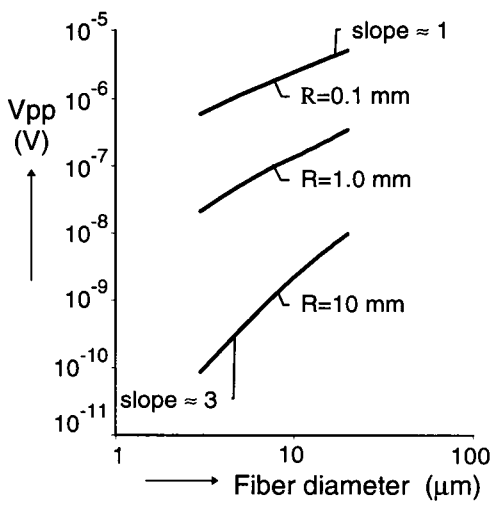

FIGURE 3 Peak-to-peak SFAP amplitude as a function of fiber diameter for three different electrode-fiber distances (R = 0.1 mm, R = 1 mm, and R = 10 mm) in an unbounded homogeneous volume conductor. The slope of the R = 0.1 mm curve is given for the large fiber diameters, and the slope of the R = 10 mm curve is given for the small fiber diameters.

Farther away from the fiber ($R \gg L$), the source has a tripolar character, resulting in $p \approx 3$.

The relationship between SFAP amplitude and fiber diameter is thus very much dependent on the recording situation, even for monopolar recordings. For multipolar recordings the slope of this relationship may be even larger than $p = 3$. This explains, qualitatively, the differences in p as reported in the literature.

Fig. 4 shows the SFAP's peak-to-peak amplitude as a function of electrode fiber distance for a fiber diameter of 10 μm. For short distances ($R \ll L$) the slope q equals -1, indicating that the amplitude is inversely proportional with distance: $\hat{s}(R) \propto R^{-1}$, which is consistent with the monopolar character of the field around a node. Halfway between two nodes $q \approx 0$ for very small distances (not shown in the figure). For $R \gg L$ the fiber has a tripolar character again: $\hat{s}(R) \propto R^{-3}$, which is the same result as obtained by Plonsey (1974) for unmyelinated fibers. These results are also similar to the results obtained by Stephanova et al. (1989), who used a model with leaking internodes. In particular, the value $q \approx -1.8$ for electrode-fiber distances between 1 and 5 mm, as reported in their publication, agrees with the results shown in Fig. 4.

Several linearities in the models, such as the linearity between fiber diameter and internodal length, the linearity between fiber diameter and nodal current, the inverse linearity between distance and potential (the Green's function for potential fields is proportional to $1/r$), and the linearity between potential and current ensure that the principle of corresponding states (Rushton, 1951) also holds for the extracellular potential in a volume conductor. If the whole geometry is scaled by a factor γ, then the corresponding SFAPs are given by

$$s(t; D, r, z) = s(t; \gamma D, \gamma r, \gamma z) \quad (9)$$

In Fig. 5 this is shown for a 10-μm-diameter fiber and an electrode-fiber distance of 2 mm, and a corresponding state:

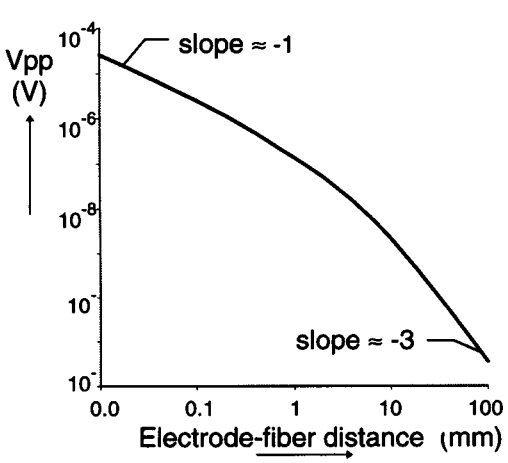

FIGURE 4 Peak-to-peak SFAP amplitude as a function of electrode-fiber distance (R) for a 10-μm-diameter fiber. The slopes of the curve are given for small and for large values of R.

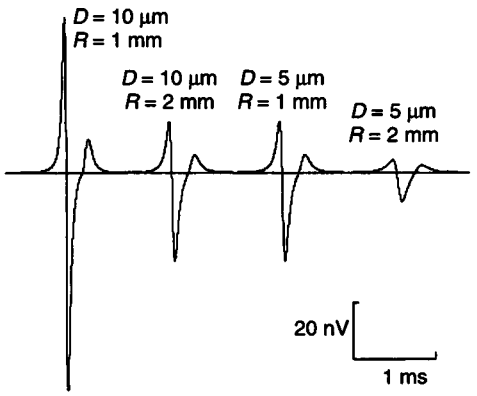

FIGURE 5 SFAPs in the unbounded homogeneous model for two different fiber diameters and two different electrode-fiber distances (indicated in the figure). The SFAPs for $D = 10$ μm, $R = 2$ mm and $D = 5$ μm, $R = 1$ mm are identical, illustrating the principle of corresponding states.

a 5-μm fiber and a distance of 1 mm. The SFAPs are identical. The result that $p = -q = 1$ for $R \ll L$ and that $p = -q = 3$ for $R \gg L$ is a direct consequence of the corresponding states principle.

For large distances and small fibers, the saltatory conduction of the action potential becomes visible in the SFAP as a small ripple with a period of exactly the conduction time of the action potential from node to node.

SFAP duration

It is difficult to assign a nonambiguous duration to a SFAP, because the shapes of the SFAPs change with the recording situation. However, the interval between the first peak and the second peak, T_{pp}, seems to be a meaningful descriptor related to the duration of the SFAP. In many models one of the basic assumptions is that the duration of the SFAP is scaled by a power of the propagation velocity v, or equivalently, when assuming linearity between v and D,

$$s(t; D) = \hat{s}(D) \cdot s_0((D/D_0)^{\lambda} \cdot t) \quad (10)$$

where s_0 is the SFAP of the fiber with diameter D_0. Just like the parameter p in Eq. 8, it turns out that λ is by no means constant over the whole range of fiber diameters, except for the recording situations very close to a single node of Ranvier ($R \ll L$), where $\lambda = 0$ and far away from the fiber ($R \gg L$), where $\lambda = 1$. For $R \ll L$ the SFAP is a copy of the action current and has a constant of $T_{pp} = 23$ μs. For $R \gg L$ the source can again be seen as a moving tripole that passes by with a velocity that is proportional to the fiber diameter, and therefore T_{pp} is inversely proportional to the fiber diameter ($\lambda = 1$). Between these extremes the behavior of T_{pp} as a function of fiber diameter is more complex in this model. Most often in the models in the literature, $\lambda = 0$ (see, e.g., Schoonhoven and Stegeman for an overview).

However, it should be noted that for many recording situations, the SFAP is not just a scaled version (in time and

amplitude) of a standard SFAP, but that its shape changes with fiber diameter.

Inhomogeneous model

Test

To test the accuracy of the numerical method, an unbounded homogeneous isotropic medium was simulated. For a 10-μm-diameter fiber with electrodes at distances of 1 mm and 50 mm in a volume conductor model of 500 × 250 mm, as described in the Methods but with all conductivities at 1.0 $(\Omega m)^{-1}$, the resulting numerical SFAPs differed from the corresponding SFAPs calculated with the unbounded homogeneous model by less than 0.1%.

Influence of cuff length on SFAP amplitude

The presence of a restriction of the extracellular space, in the form of a cuff electrode, has a strong influence on the amplitude of the SFAP. In Fig. 6 the peak-to-peak amplitudes of SFAPs of a 10-μm-diameter fiber are shown for a cuff with 1.0-mm radius and variable length, and with a ring electrode in the middle of the cuff. For this fiber the maximum amplitude is ~1.7 μV, which is reached for a cuff length of at least 28 mm. This amplitude is 12.5 times higher than the one without a cuff (homogeneous medium). The obtained minimum length (28 mm) for maximum amplitude is at the low end of experimentally measured optimal lengths (Stein et al., 1975; Hoffer, 1990), but the active fibers in those experiments are probably thicker than 10 μm, whereas the optimal length is approximately proportional to the fiber diameter.

The presence of a nerve bundle, with a radius of 0.55 mm (including the perineurium) around the active fiber, changes the amplitude of the calculated SFAP. For large cuff lengths the amplitude is increased slightly (3%), which can be explained by the fact that the current is mainly (although not entirely) axial, and then the factor $R_e/(R_e + R_a)$ in Eq. 6 comes into play, where, according to Eq. 7, the R_e's are different for the situations with and without a nerve bundle. However, according to this one-dimensional analysis the difference should have been 18% instead of the observed 3% in the inhomogeneous model.

For smaller cuff lengths (<15 mm) the presence of the bundle decreases the peak-to-peak amplitude. In the case shown in Fig. 6 the difference is quite large. However, if there is connective tissue growth inside the cuff the result may be different.

Influence of cuff length on SFAP duration

The peak-to-peak interval (T_{pp}) increases linearly with cuff length, except for very small cuff lengths or large diameters. This proportionality can be derived directly from Eq. 6 for the situations in which this equation is valid. For long and narrow cuffs Eq. 6 gives $T_{pp} = z/v$, where z is the electrode position in the cuff relative to the cuff end at which the signal enters the cuff. For an electrode in the center this yields $T_{pp} = L_{cuff}/v$. Fig. 9 *a*, the trace for z = 50 mm, illustrates this. The first positive peak occurs when the action potential enters the cuff, the second (negative) peak occurs when the AP passes the electrode, and when the AP leaves the cuff a third and positive phase is seen. For a long cuff, these phases are separated, whereas for a shorter cuff (e.g., in Fig. 9, *b* and *c*) the phases are superimposed to give the characteristic triphasic signal. For further interpretation see the Discussion.

Influence of cuff diameter and radial electrode position

In Fig. 7 the peak-to-peak amplitudes of a 10-μm-diameter fiber are given as a function of cuff radius, for a cuff length of 20 mm. For comparison, the result of the homogeneous model is given in the same figure, where "cuff radius" is to be read as "electrode-fiber distance." If the electrode is kept

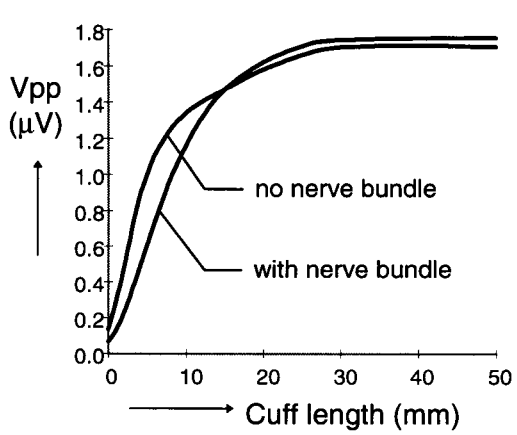

FIGURE 6 Peak-to-peak SFAP amplitudes as a function of cuff length for a 10-μm-diameter fiber and a cuff radius of 1 mm. Two curves are shown: one for the case with no nerve bundle and one for the case in which a nerve bundle is present in the model.

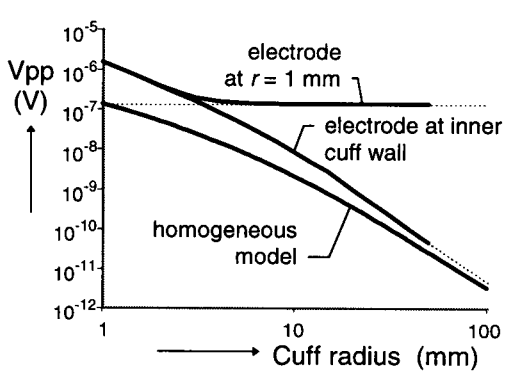

FIGURE 7 Peak-to-peak SFAP amplitudes as a function of cuff radius for a 10-μm-diameter fiber and a cuff length of 20 mm. For the upper curve the electrode is at 1 mm radius, and for the middle curve the electrode is at the inner cuff wall. For comparison, V_{pp} is also shown as a function of electrode-fiber distance in the unbounded homogeneous model.

at a distance of 1 mm from the fiber, and the cuff radius is increased, then it is seen that, for a radius of more than 8 mm, the presence of the cuff has a negligible influence as compared to the homogeneous model with a 1 mm electrode fiber distance. Up to a radius of approximately 2 mm the position of the electrode (at 1 mm or at the inner cuff wall) does not have a significant effect on the recorded signal. Above 2 mm the effect becomes apparent.

If the electrode is at the inner cuff wall, then the peak-to-peak amplitude slowly approaches the amplitude, as calculated in the homogeneous model, but up to a radius of 100 mm a small difference is still seen. For large cuff diameters V_{pp} is proportional to R^{-3}, just as in the homogeneous model.

For smaller diameters V_{pp} is proportional to R^{-2}, which is in agreement with experimental results from Davis et al. (1978) and with the one-dimensional model (see Discussion).

Axial electrode position

According to Eq. 6 the SFAP amplitude depends on the axial position of the electrode in the cuff. The equation predicts that at the cuff ends ($z = 0$ or $z = L_{cuff}$) the SFAP vanishes. This result is an anomaly because of the boundary condition (zero potential at the cuff ends). However, Fig. 8 shows that at the proximal end of a 100-mm-long cuff with a 1-mm radius the SFAP amplitude is indeed much lower than in the center of the cuff (0.13 μV versus 1.8 μV, which gives almost a factor 14 between these two cases).

Fig. 8 also shows that the peak-to-peak amplitude is at maximum not at the center, but at ~15 mm (in the case of a long cuff) from the proximal end. This is because the first peak first increases in amplitude and then decreases again, in favor of the third peak. The amplitude of the second peak (V_p in Fig. 8) remains constant from 15 mm from the proximal end to the center of the cuff.

Fig. 9 shows the shapes of the SFAPs for a 100-mm-long cuff and for 20-mm and 5-mm-long cuffs as well, at different axial electrode positions (*solid lines*). The difference between the proximal end and the distal end is notable.

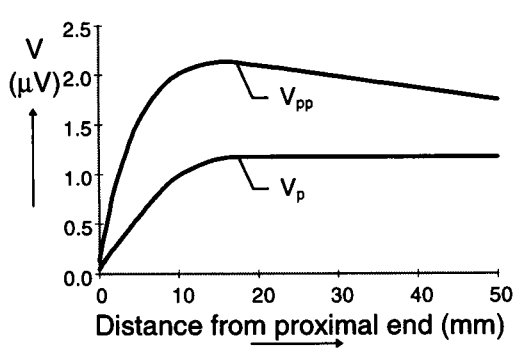

FIGURE 8 Peak-to-peak SFAP amplitude and the negative peak amplitude as a function of electrode position (distance from the proximal cuff end) for a 10-μm-diameter fiber, a cuff length of 100 mm, and cuff radius of 1 mm.

Cuff conductivity

In Fig. 10 the relationship between the peak-to-peak amplitude and the cuff conductivity, as a simulation of a leaking gap in the cuff, is shown. The gap conductivity was 1.0 $(\Omega m)^{-1}$, the same as for the extracellular medium. According to Fig. 10, the effect of the cuff becomes just visible at about a conductivity of 0.001 $(\Omega m)^{-1}$, and the SFAP amplitude is reduced by 50% at a conductivity of 0.01 $(\Omega m)^{-1}$, the latter corresponding to a gap width of only 63 μm (following from Eq. 2) for this cuff with a 1.0-mm radius. This result shows the importance of a hermetic sealing of the cuff.

Fiber diameter

In Fig. 11 the peak-to-peak amplitude is shown as a function of fiber diameter for a 20-mm-long cuff with a 1-mm radius. For comparison, the curve from the homogeneous model for an electrode fiber distance of 1 mm is shown again (copied from Fig. 3). The average slope of the curves is 1.2 for the homogeneous model and 1.6 and 1.8 for the models with a cuff and no nerve bundle, and with both a cuff and a nerve bundle, respectively. This higher slope for the cases with a cuff present implies that the cuff emphasizes the signals from large fibers as compared with the homogeneous case.

A comparison of the case of a 10-μm-diameter fiber and 10-mm-long cuff with radius 1 mm with the case of a 20-μm diameter fiber and a 20-mm-long cuff with radius 2 mm showed that the resulting SFAPs were identical, confirming the principle of corresponding states being valid for the inhomogeneous model as well.

One-dimensional model

For a 10-μm-diameter fiber in a cuff of 1-mm radius and 100-mm length, and with no nerve bundle, the SFAP obtained according to the one-dimensional analysis (Eq. 6) was only 3% different from the one calculated in the inhomogeneous model. At a cuff length of 2 mm (two internodal lengths) the difference was 11%. With a nerve bundle, and the extracellular resistance calculated according to Eq. 7, the difference was ~15% for a 100-mm-long cuff, and already more than 50% for a cuff length of 5 mm.

For cuffs with larger radii, the differences increased considerably: up to a 2-mm radius the difference with the inhomogeneous model was less than 3% (no nerve bundle), and it increased to 15% at a 4-mm radius and 84% at 10 mm (but at these large radii Stein and Pearson's model assumptions were violated).

If the electrode was placed 1 mm from the cuff end of a 100-mm-long cuff with 1-mm radius (no nerve bundle), the difference between the models was more than 50%, and this difference dropped to 3.3% at 5 mm from the cuff end.

In Fig. 9 some of the "one-dimensional" SFAPs are shown (*dotted lines*), together with the SFAPs as calculated with the inhomogeneous volume conductor (*solid lines*). It

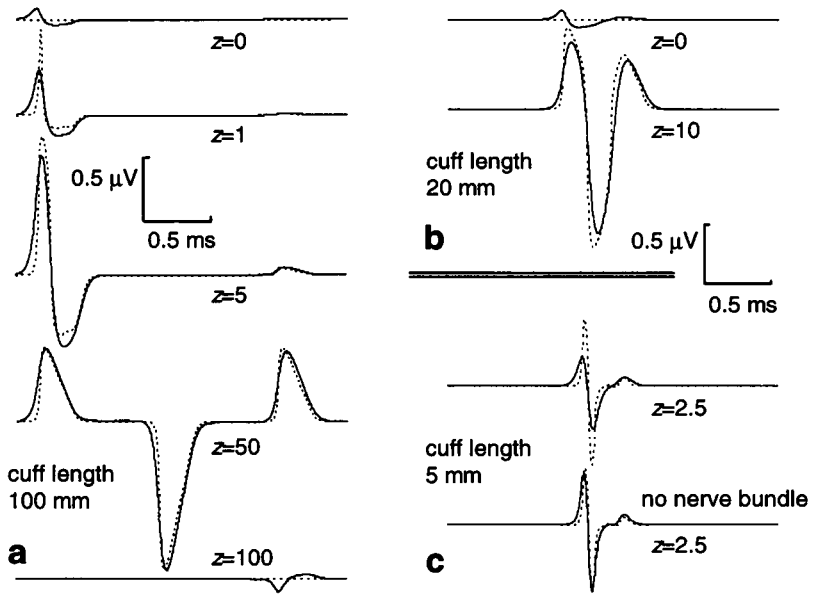

FIGURE 9 SFAP waveforms for different cuff lengths and different axial electrode positions (z). In all cases the fiber diameter is 10 μm and the cuff radius is 1 mm, and a nerve bundle is incorporated into the model, except for the lower trace in c, where there is no nerve bundle. ——, Waveforms calculated in the inhomogeneous model; ·····, waveforms from the one-dimensional model. (a) Cuff length 100 mm; (b) Cuff length 20 mm; (c) Cuff length 5 mm.

can be seen that the peak-to-peak amplitude is probably not the best measure with which to evaluate the accuracy of the one-dimensional analysis. For example, in Fig. 9 a, for an electrode 5 mm from the proximal end, the V_{pp}'s differ by 4%, but the individual peaks show much larger differences.

DISCUSSION AND CONCLUSIONS

The material presented in this paper focuses on single fiber action potentials in a relatively simple volume conductor and with monopolar electrodes. The model is easy to extend to compound action potentials in more complicated volume conductors, and with multipolar electrodes. Moreover, the model is flexible: it is easy to change parameters such as fiber diameter, conductivities, volume conductor geometry, and electrode positions and configurations. The same principles underlying the symmetrical model can also be applied to true three-dimensional volume conductor models, although potential field calculations will then be much more time consuming.

The fiber model was simplified to a collection of point sources (the nodes of Ranvier), after the nodal transmembrane current was calculated in a fiber model with nonleaking internodes. This omission of the internodes may influence the potential field at distances on the order of the fiber diameter, but for larger distances, as for the cuff electrodes studied here, the effect is negligible. An important argument for the validity of this approach is that the overall behavior of the fiber is not changed by leaving out the myelin leakage (Goldman and Albus, 1968). Moreover, the amplitude versus electrode-fiber distance relationship obtained in the present study was in agreement with the results reported by Stephanova et al. (1989), who did use a model with leaking internodes. The amount of work involved in SFAP computation is enormously reduced by regarding the fiber as a collection of discrete sources instead of a continuous line source, which is an important advantage, especially when

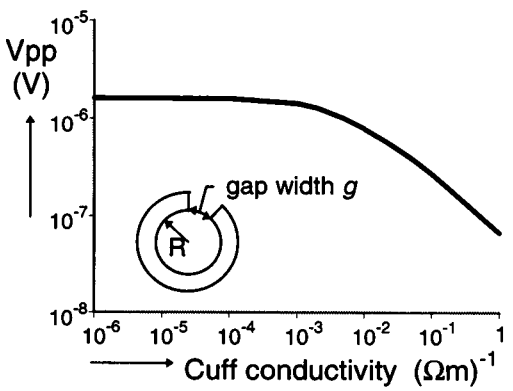

FIGURE 10 Peak-to-peak SFAP amplitude as a function of cuff conductivity. The inset shows the definition of gap width, which can be related to the conductivity (see Inhomogeneous Volume Conductor in Methods section).

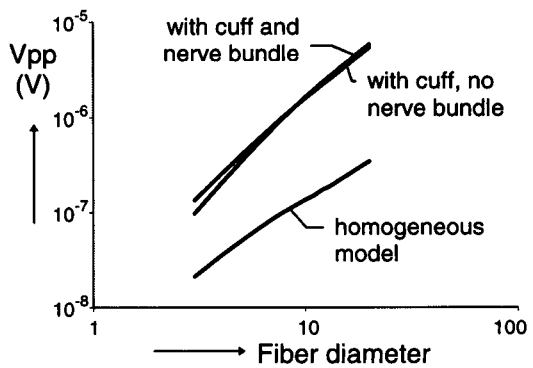

FIGURE 11 Peak-to-peak SFAP amplitudes as a function of fiber diameter for a 20-mm-long cuff with radius 1 mm. V_{pp} is shown for three different cases, as indicated in the figure.

the method is used for the calculation of compound action potentials.

For very small and for very large electrode fiber distances in the homogeneous model, the SFAP waveform has a more or less constant shape for different fiber diameters. In that case the SFAP amplitude and SFAP duration can be parameterized by the fiber diameter (see Eqs. 8 and 10). For less extreme distances the shape also depends on fiber diameter, in such a way that the principle of corresponding states holds (if the whole world geometry is scaled with a single factor, the SFAP does not change). The exponents p and λ were found to vary between 0 and 3 for p and 0 and 1 for λ. This explains the large variation as seen in the literature. An important point is that these parameters follow from the model and are not part of the model assumptions.

The influence of cuff length on SFAP amplitude was investigated and found to be in accordance with experimental results reported in the literature (Stein et al., 1975; Hoffer, 1990). Because, according to the one-dimensional model, the triphasic signal can be regarded as the superposition of three monophasic signals, where the first phase arises at the moment the AP enters the cuff, the second phase arises when the AP travels past the electrode, and where the third phase arises when the AP leaves the cuff (as illustrated in Fig. 9), the time interval between the peaks, and thus also T_{pp}, increases indefinitely with cuff length. For long cuffs the cuff can also be regarded differently: upon entry (and leaving) the AP shows up as a voltage source at one of the cuff ends, because of the low resistivity outside the cuff. The (high) resistance between this cuff end and the electrode, together with the resistance between the electrode and the second cuff end, then forms a voltage divider. This view yields exactly the same relative amplitudes for the first and the third phases as the one-dimensional model: z/L_{cuff} and $(1 - z)/L_{cuff}$, in agreement with Eq. 6.

The influence of cuff diameter on SFAP amplitude was different from the relationship found by Stein and Oguztöreli (1978). For a cuff radius of 10 mm at a cuff length of 20 mm, the peak-to-peak amplitude decreased as $\sim R^{-2.5}$, which is quite different from $R^{-1.2}$, obtained by Stein and Oguztöreli. Here, probably the effect of an applied voltage at the external surface of the fiber instead of a current source becomes apparent (see Heringa et al., 1989, for a discussion on this topic). However, repeating their calculations for very large values ($R \gg 10$ mm) of the cuff diameter, the exponent becomes extremely large, going to minus infinity instead of the theoretical -3 for very large R, probably as a result of the boundary conditions of zero voltage at the cuff ends.

For small cuff radii (up to a few millimeters) the volume conduction model showed a signal amplitude that decreased as $\sim R^{-2}$ for increasing R. For small cuff radii the one-dimensional model is also valid, and, according to Eqs. 6 and 7, assuming that $R_e \ll R_a$, the one-dimensional model also gives this R^{-2} relationship, because R_e is proportional to R^{-2}. Experimental evidence supports this finding as well: Davis et al. (1978) reported CAP peak-to-peak amplitudes of 2.29, 1.24, and 0.75 mV for 20-mm-long cuffs with radii of 1.0, 1.3, and 1.7 mm, respectively, which agrees with the R^{-2} relationship for SFAPs in the models.

The axial position of the electrode in the cuff was shown to be important. At a distance of 1 mm from the cuff ends, the SFAP amplitude was only 25% of the amplitude recorded in the center of the cuff. This percentage was the same as recorded by Thomsen et al. (manuscript submitted for publication) with a 22-mm-long cuff electrode around the tibial nerve of the rabbit, where the outer electrodes were $\sim$1 mm from the cuff ends.

The radial position of the electrode was not so important as long as the cuff radius was not too large. The cuff makes the field more homogeneous, i.e., the radial decline of the field around the fiber is much less than it would be without a cuff. This implies that the position of the nerve fiber inside the nerve is less important in the case where a cuff is present than when there is no cuff.

From the simulations with the different cuff conductivities it was shown that even a small opening along the cuff length strongly affects the amplitude of the SFAP. However, this result is more qualitative than quantitative, because a gap was simulated as a distributed higher cuff conductivity. In a true three-dimensional situation the current distribution will be different, which will affect the numbers given in the results.

The influence of the presence of a nerve bundle was quite strong for small cuff lengths (<15 mm) with lower SFAP amplitudes for the smaller cuff lengths and slightly higher for the longer cuffs, as compared with the model without a nerve bundle. The one-dimensional analysis showed a higher amplitude with the nerve bundle for all cuff lengths, thus yielding large differences with the inhomogeneous model for short cuffs. For the case without a nerve bundle, the one-dimensional results were remarkably good for cuff lengths down to 3 mm and cuff radii up to 2 mm. For other situations and for different cuff geometries, a more advanced model, such as the one presented in this paper, is indispensible.

APPENDIX A: THE TIME INTEGRAL OF THE NODAL ACTION CURRENT AND THE SINGLE FIBER ACTION POTENTIAL

The time integral of the action current equals zero

For an idealized, infinitely long myelinated nerve fiber, the action current, $i_n(t)$, has a constant node-to-node delay, T. The shape of the AC is thus restricted according to $i_n(t) = i_0(t - nT)$. A second restriction on the shape of the AC is that it has finite power, and therefore $i_n(t)$ can be integrated over an infinite time interval. The time integral Int_n of $i_n(t)$ can be written as

$$\mathrm{Int}_n = \int_{-\infty}^{\infty} i_n(t)\mathrm{d}t = \int_{-\infty}^{\infty} i_0(t - nT)\mathrm{d}t = \int_{-\infty}^{\infty} i_0(t)\mathrm{d}t = \mathrm{Int}_0 \tag{A.1}$$

The sum of the integrated ACs of all nodes of the fiber can be written as

$$\sum \mathrm{Int_n} = \lim_{N\to\infty}(N \cdot \mathrm{Int_0}) \tag{A.2}$$

where N is the number of nodes. Alternatively, Eq. A.1 gives rise to a summation:

$$\sum \mathrm{Int_n} = \sum_{n=-\infty}^{\infty}\left(\int_{-\infty}^{\infty} i_n(t)\mathrm{d}t\right)$$

which can be rewritten as

$$\sum \mathrm{Int_n} = \int_{-\infty}^{\infty}\left(\sum_{n=-\infty}^{\infty} i_n(t)\right)\mathrm{d}t$$

Because the nodes of Ranvier are the only sources and sinks in the (resistive) volume conductor, the net current must be zero at any instant. Therefore the summation (the integrand) in the latter expression must be zero. Thus:

$$\sum \mathrm{Int_n} = 0 \tag{A.3}$$

From Eq. A.3 we can immediately conclude that Eq. A.2 can only be true if $\mathrm{Int_0} = 0$. Equation A.1 then finally gives the important result that the time integral of the action current vanishes:

$$\mathrm{Int_n} = \int_{-\infty}^{\infty} i_n(t)\mathrm{d}t = 0 \tag{A.4}$$

It is not difficult to prove a similar result for unmyelinated nerve fibers by changing the summations into integrals, and then following the same procedure.

The time integral of the SFAP equals zero

A single fiber action potential, $s(t)$, can be regarded as being the superposition of potentials resulting from the currents $i_n(t)$ at each of the nodes:

$$s(t) = \sum_{n=-\infty}^{\infty} w_n i_n(t) \tag{A.5}$$

where w_n is a weight function that depends solely on the volume conductor. The time integral of the SFAP is now given by

$$\int_{-\infty}^{\infty} s(t)\mathrm{d}t = \int_{-\infty}^{\infty}\left(\sum_{n=-\infty}^{\infty} w_n i_n(t)\right)\mathrm{d}t = \sum_{n=-\infty}^{\infty} w_n\left(\int_{-\infty}^{\infty} i_n(t)\mathrm{d}t\right) \tag{A.6}$$

Using Eq. A.4 for the integral on the right-hand side of Eq. A.6, we arrive at

$$\int_{-\infty}^{\infty} s(t)\mathrm{d}t = 0 \tag{A.7}$$

meaning that the time integral of the SFAP evaluates to zero, independently of the electrode configuration and the volume conductor. This result is counterintuitive, because many SFAPs used in the literature do not integrate to zero (e.g., Erlanger and Gasser, 1937; Gu et al., 1996), which is most pronounced for signals at the surface or boundary of a volume conductor (Heringa et al., 1989; Gu et al., 1996). Both the volume conductor model as presented in this work and the one-dimensional model (Eq. 6) yield SFAPs that integrate to zero.

The monophasic unmyelinated SFAP also integrates to zero

The result, Eq. A.7, seems to contradict the results of Heringa et al. (1989), who showed that at the boundary of an infinitely long radial restriction the SFAP of an unmyelinated fiber is monophasic. However, this "monophasic" SFAP is a limit case of a triphasic SFAP. The first and the third phases are infinitely far away in this case, but the time integral still vanishes. This can be proved simply by taking the expression for the field (equation 10 in Heringa et al., 1989) and integrating it with respect to z (note that, in this case, the z and t coordinates can be interchanged).

Usually, when cylindrical coordinates are used, the SFAP can be given in the following form (the formulation by Heringa et al. (1989) is also in this form):

$$\phi(\rho, z) = \int_{-\infty}^{\infty} G(k)W(\rho, k)e^{\mathrm{i}kz}\mathrm{d}k \tag{A.8}$$

where $G(k)$ is the Fourier transform of the (continous) action current $g(z)$, and $W(\rho, k)$ is the Fourier transform of a weight function, $w(\rho, z)$, which describes the effect of the volume conductor. The action current $g(t)$ is subject to a restriction similar to that of the AC of the myelinated fiber. In other words, the net AC is zero:

$$\int_{-\infty}^{\infty} g(z)\mathrm{d}z = 0 \tag{A.9}$$

Because the product GW in the (spatial) frequency domain and the convolution (g^*w) in the spatial domain are Fourier transform pairs, Eq. A.8 can be written as

$$\phi(\rho, z) = \int_{-\infty}^{\infty} g(z-\zeta)w(\rho, \zeta)\,\mathrm{d}\zeta \tag{A.10}$$

Integrating Eq. A.10 for z gives

$$\begin{aligned}\int_{-\infty}^{\infty}\phi(\rho, z)\mathrm{d}z &= \int_{-\infty}^{\infty}\int_{-\infty}^{\infty} g(z-\zeta)w(\rho, \zeta)\,\mathrm{d}\zeta\,\mathrm{d}z \\ &= \int_{-\infty}^{\infty} w(\rho, \zeta)\left(\int_{-\infty}^{\infty} g(z-\zeta)\,\mathrm{d}z\right)\mathrm{d}\zeta\end{aligned} \tag{A.11}$$

Because $g(z)$ vanishes for large positive and negative values of z, the inner integral on the right-hand side of Eq. A.11 can be replaced by $\int_{-\infty}^{\infty} g(\rho, z)\,\mathrm{d}z = 0$, according to Eq. A.9. Therefore, the whole right-hand side of Eq. A.11 becomes zero:

$$\int_{-\infty}^{\infty}\phi(\rho, z)\mathrm{d}z = 0 \tag{A.12}$$

In many practical cases the integral will not seem to be zero, and a monophasic SFAP is recorded. This can be illustrated with the SFAP shown in Fig. 9 *a* for a 100-mm-long cuff and the electrode in the middle (z = 50 mm). For even longer cuffs or other kinds of long restrictions of

the extracellular space, and with a limited time window around the negative peak, the SFAP looks monophasic indeed.

APPENDIX B: FIBER EQUATIONS

For a myelinated fiber with a nonleaking internode and a negligible extracellular resistance as compared with the intraaxonal resistance, the transmembrane potential V_n at node n is given by

$$\frac{dV_n}{dt} - \frac{d}{4\rho_a c_m \ell L}(V_{n-1} - 2V_n + V_{n+1}) + \frac{1}{c_m}(I_{Na} + I_L) = 0 \tag{B.1}$$

The total nodal current I_n at node n is the sum of the capacitive current and the ionic currents:

$$I_n = c_m \pi d\ell \frac{dV_n}{dt} + \pi d\ell (I_{Na} + I_L)$$

$$= G_a(V_{n-1} - 2V_n + V_{n+1}) \tag{B.1}$$

where $G_a = \pi d^2/4\rho_a L$ is the internodal intraaxonal conductance. Because d/L is constant, and $V_{n-1} - 2V_n + V_{n+1}$ is independent of d as well, it follows from Eq. B.2 that the transmembrane current I_n is linear with d. The sodium current I_{Na} and the leakage current I_L are given as:

$$I_{Na} = \bar{g}_{Na} h m^2 (E - E_{Na})$$

$$I_L = g_L(E - E_L)$$

where

$$dm/dt = \alpha_m(1 - m) - \beta_m m, \qquad m(0) = 0.00331$$

$$dh/dt = \alpha_h(1 - h) - \beta_h h, \qquad h(0) = 0.7503$$

$$E = V + V_{rest}\ (\text{mV})$$

$$\alpha_m = (0.363E + 126)/[1 + \exp((-49 - E)/5.3)]$$

$$\beta_m = \alpha_m/\exp((E + 56.2)/4.17)$$

$$\alpha_h = \beta_h/\exp((E + 74.5)/5)$$

$$\beta_h = 15.6/[1 + \exp((-56 - E)/10)]$$

The parameters are

ρ_a	intra-axonal resistivity (0.7 Ωm)
c_m	membrane capacitivity (0.02 F/m^2)
g_{Na}	maximum sodium conductivity (14.45 · 10^3 1/(Ωm)^2)
g_L	leakage conductivity (1.28 · 10^3 1/(Ωm)^2)
E_{Na}	sodium equilibrium potential (35.64 mV)
E_L	leakage equilibrium potential (−80.11 mV)
V_{rest}	membrane resting potential (−80.0 mV)
D	fiber diameter (variable: 3–20 μm)
d	axon diameter (0.6D)
l	length of node of Ranvier (1.5 μm)
L	length of the internode (100D)

APPENDIX C: VOLUME CONDUCTOR EQUATIONS

Equation 2 can be discretized on a grid as shown in Fig. 12. Define:

$$\begin{cases} \tau^r_{ij} = \dfrac{h_{i-1}\sigma^r_{i-1j} + h_i\sigma^r_{ij}}{h_{i-1} + h_i} \\ \tau^z_{ij} = \dfrac{k_{j-1}\sigma^z_{ij-1} + k_j\sigma^z_{ij}}{k_{j-1} + k_j} \end{cases} \tag{C.1}$$

Then the derivatives in Eq. 2 can be approximated as

$$\begin{cases} \left[\dfrac{\partial}{\partial r}\left(\sigma_r \dfrac{\partial}{\partial r}\right) + \dfrac{1}{r}\sigma_r \dfrac{\partial}{\partial r}\right]_{ij} \approx a_{ij}u_{ij-1} + b_{ij}u_{ij+1} - (a_{ij} + b_{ij})u_{ij} \\ a_{ij} = \dfrac{\tau^r_{ij-1}}{k_{j-1}}\left(\dfrac{2}{(k_{j-1} + k_j)} - \dfrac{1}{2r_j}\right) \\ b_{ij} = \dfrac{\tau^r_{ij}}{k_j}\left(\dfrac{2}{(k_{j-1} + k_j)} + \dfrac{1}{2r_j}\right) \end{cases} \tag{C.2}$$

$$\begin{cases} \left[\dfrac{\partial}{\partial z}\left(\sigma_z \dfrac{\partial u}{\partial z}\right)\right]_{ij} \approx c_{ij}u_{i-1j} + d_{ij}u_{i+1j} - (c_{ij} + d_{ij})u_{ij} \\ c_{ij} = \dfrac{2\tau^z_{i-1j}}{h_{i-1}(h_{i-1} + h_i)} \\ d_{ij} = \dfrac{2\tau^z_{ij}}{h_i(h_{i-1} + h_i)} \end{cases} \tag{C.3}$$

$$\begin{cases} \left[\dfrac{I_n(t)}{2\pi r_n}\delta(r - r_n, z - z_n)\right]_{ij} \approx e_{ij}I_{ij} \\ e_{ij} = \dfrac{2}{(h_{i-1} + h_i)(k_{j-1} + k_j)\pi r_j} \end{cases} \tag{C.4}$$

Combining Eq. 2 with Eqs. C.1–C.4 gives

$$u_{ij} = \frac{a_{ij}u_{ij-1} + b_{ij}u_{ij+1} + c_{ij}u_{i-1j} + d_{ij}u_{i+1j} - e_{ij}I_{ij}}{a_{ij} + b_{ij} + c_{ij} + d_{ij}} \tag{C.5}$$

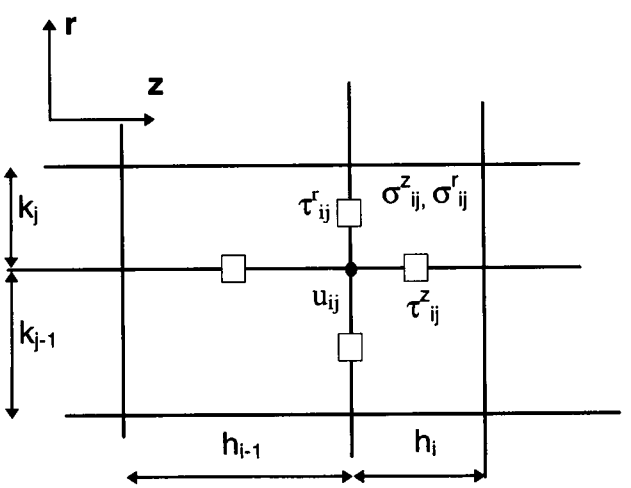

FIGURE 12 Definition of grid parameters and conductivities.

Because of cylindrical symmetry, the axis can be taken as the lower boundary of the model, with a boundary condition that there is no current perpendicular to the boundary. This was implemented by taking $u_{ij-1} = u_{ij+1}$, and $a_{ij} = b_{ij}$ in Eq. C.5.

This work was supported by the Danish National Research Council.

REFERENCES

Barker, A. 1981. Nerve conduction velocity distributions: an iterative method using two compound action potentials recorded from the same site. *In* Conduction Velocity Distributions. L. J. Dorfman, K. L. Cummins, and L. J. Leifer, editors. Alan R. Liss, New York. 137–180.

Buchthal, F., and A. Rosenfalck. 1966. Evoked action potentials and conduction velocity in human sensory nerves. *Brain Res.* 3:1–122.

Chiu, S. Y., J. M. Ritchie, R. B. Rogart, and D. Stagg. 1979. A quantitative description of membrane currents in rabbit myelinated nerve. *J. Physiol. (Lond.).* 292:149–166.

Davis, L. A., T. Gordon, J. A. Hoffer, J. Jhamandas, and R. B. Stein. 1978. Compound action potentials recorded from mammalian peripheral nerves following ligation or resuturing. *J. Physiol. (Lond.).* 285: 543–559.

Erlanger, J., and H. S. Gasser. 1937. Electrical Signs of Nervous Activity. University of Pennsylvania Press, Philadelphia.

FitzHugh, R. 1962. Computation of impulse initiation and saltatory conduction in a myelinated nerve fiber. *Biophys. J.* 2:11–21.

Ganapathy, N., and J. W. Clark. 1987. Extracellular currents and potentials of the active myelinated nerve fiber. *Biophys. J.* 52:749–761.

Goldman, L., and J. S. Albus. 1968. Computation of impulse conduction in myelinated fibers: theoretical basis of the velocity-diameter relation. *Biophys. J.* 8:596–607.

Goodall, E. V., L. M. Kosterman, J. Holsheimer, and J. J. Struijk. 1995. Modeling study of activation and propagation delays during stimulation of peripheral nerve fibers with a tripolar cuff electrode. *IEEE Trans. Rehab. Eng.* 3:272–282.

Gu, D., R. E. Gander, and E. C. Crichlow. 1996. Determination of nerve conduction velocity distribution from sampled compound action potentials. *IEEE Trans. Biomed. Eng.* 43:829–838.

Haugland, M. K., and T. Sinkjaer. 1995. Cutaneous whole nerve recordings used for correction of footdrop in hemiplegic man. *IEEE Trans. Rehab. Eng.* 3:307–317.

Heringa, A., D. F. Stegeman, and J. P. C. de Weerd. 1989. Calculated potential and electric field distributions around an active nerve fiber. *J. Appl. Phys.* 66:2724–2731.

Hermann, L. 1881. Untersuchungen über die Actionsströme des Nerven. II. *Pflüger's Arch. Gesamte Physiol.* 24:246–294.

Hoffer, J. A. 1975. Long-Term Peripheral Nerve Activity during Behaviour in the Rabbit: The Control of Locomotion. Publication no. 76-8530. University Microfilms, Ann Arbor, MI.

Hoffer, J. A. 1990. Techniques to study spinal-cord, peripheral nerve, and muscle activity in freely moving animals. *In* Neuromethods, Vol. 15, Neurophysiological Techniques: Applications to Neural Systems. A. A. Boulton, G. B. Baker, and C. H. VanderWolf, editors. The Humana Press, Inc., Clifton, N. J. 65–145.

Hursh, J. B. 1939. Conduction velocity and diameter of nerve fibers. *Am. J. Physiol.* 127:131–139.

Lorente de Nó, R. 1947. A study of nerve physiology. *Stud. Rockefeller Inst. Med. Res.* 132:384–477.

Malmivuo, J., and R. Plonsey. 1995. Bioelectromagnetism: Principles and Applications of Bioelectric and Biomagnetic Fields. Oxford University Press, Oxford.

Marks, W. B., and G. E. Loeb. 1976. Action currents, internodal potentials, and extracellular records of myelinated mammalian nerve fibers derived from node potentials. *Biophys. J.* 16:655–668.

Olsen, W. H., and S. L. BeMent. 1981. Compound action potential reconstructions and predicted fiber diameter distributions. *In* Conduction Velocity Distributions. L. J. Dorfman, K. L. Cummins, and L. J. Leifer, editors. Alan R. Liss, New York. 57–83.

Plonsey, R. 1964. Volume conductor fields of action currents. *Biophys. J.* 4:317–328.

Plonsey, R. 1974. The active fiber in a volume conductor. *IEEE Trans. Biomed. Eng.* 21:371–381.

Rijkhoff, N. J. M., J. Holsheimer, E. L. Koldewijn, J. J. Struijk, P. E. V. van Kerrebroeck, F. M. J. DeBruyne, and H. Wijkstra. 1994. Selective stimulation of sacral nerve roots for bladder control: a study by computer modeling. *IEEE Trans. Biomed. Eng.* 41:413–424.

Rosenfalck, A., and P. Ottosen. 1982. Model simulation of nerve action potentials. *Proc. World Congr. Med. Phys. Biomed. Eng.* 8:27.

Rushton, W. A. H. 1951. A theory of the effects of fibre size in medullated nerve. *J. Physiol.* 115:101–122.

Schoonhoven, R., and D. F. Stegeman. 1991. Models and analysis of compound nerve action potentials. *Crit. Rev. Biomed. Eng.* 19:47–111.

Stein, R. B., D. Charles, L. Davis, J. Jhamandas, A. Mannard, and T. R. Nichols. 1975. Principles underlying new methods for chronic neural recording. *J. Can. Sci. Neurol.* 235–244.

Stein, R. B., and M. N. Oguztöreli. 1978. The radial decline of nerve impulses in a restricted cylindrical extracellular space. *Biol. Cybern.* 28:159–165.

Stein, R. B., and G. K. Pearson. 1971. Predicted amplitude and form of action potentials recorded from unmyelinated nerve fibres. *J. Theor. Biol.* 32:539–558.

Stephanova, D., N. Trayanova, A. Gydikov, and A. Kossev. 1989. Extracellular potentials of a single myelinated nerve fiber in an unbounded volume conductor. *Biol. Cybern.* 61:205–219.

Struijk, J. J., J. Holsheimer, G. G. van der Heide, and H. B. K. Boom. 1992. Recruitment of dorsal column fibers in spinal cord stimulation: influence of collateral branching. *IEEE Trans. Biomed. Eng.* 39:903–912.

Sweeney, J. D., J. T. Mortimer, and D. Durand. 1987. Modeling of mammalian myelinated nerve for functional neuromuscular stimulation. *In* 9th Annual Conference of the Engineering Medicine and Biology Society. IEEE, New York. 1577–1578.

Trayanova, N., C. S. Henriquez, and R. Plonsey. 1990. Limitations of approximate solutions for computing the extracellular potential of single fibers and bundle equivalents. *IEEE Trans. Biomed. Eng.* 37:22–35.

Wijesinghe, R. S., F. L. H. Gielen, and J. P. Wikswo. 1991. A model for compound action potentials and currents in a nerve bundle. I. The forward calculation. *Ann. Biomed. Eng.* 19:43–72.